16th Australasian Fluid Mechanics Conference
Crown Plaza, Gold Coast, Australia
2-7 December 2007

An Experimental Investigation of Perturbations on Vortex Breakdown over Delta Wings

S. Srigrarom and M. Ridzwan

School of Mechanical and Aerospace Engineering, Nanyang Technological University (NTU)

50 Nanyang Avenue, 639798, Singapore. E-mail: mssrigrarom@ntu.edu.sg

Abstract

An experimental investigation on vortex breakdown on delta wings at high angles of attack is presented. As suggested by previous works, perturbations are used to change the platform of the delta wings to reduce the detrimental effects of vortex breakdown brought about by the Self-Induction Theory. Different patterns of 'round' perturbations are tested to obtain the favourable lift and drag characteristics for each wing. With the best pattern identified later, optimization of the shape of perturbation is explored to further improve the results. 'Teardrop' and 'diamond' perturbations are introduced as basis of comparison. Force measurements were conducted over a range of $\alpha = 0$ to 40° to justify the concept of surface shaping and evaluate its effectiveness. Dye flow visualization were used to obtain sectional views of the leading-edge vortices as they break down for a series of delta wings having sweep angles of 60°, 65° and 70°. The wings are tested constantly at a low speed of $U_\infty = 0.05$ m/s in a water tunnel facility.

A combination of side and plan views provides information on the three-dimensional nature of the vortex structure before, during and after breakdown. Details of the flow at α =15° for every wing are identified in still photographs while the dynamic characteristics of the breakdown process are examined from recorded high-speed movies. The force measurement supported by the flow visualization shows that certain combinations of perturbations indeed provide encouraging results. For wings with perturbations, generally, the vortex structure transforms from a linear structure to a wavy or "kink" structure which effectively delay or even suppress vortex breakdown. Various results have shown an increase of approximately 10% in lift characteristics and delay of stall angle for certain scenarios. The best results have been for the 60° wing where the 'teardrop' bulge in a mild perturbation pattern managed to improve lift characteristics by about 15% over the whole range of angle of attack for the tests. Results for the 65° wing and 70° wing are generally positive with the 'teardrop' perturbation again providing the best results, however with existence of discrepancies over certain angles of attack.

Introduction

The Highly swept wings, commonly called delta wings due to their triangular platform, are used in a variety of aerospace vehicles. Their usage varies from modern combat aircraft to miniscule unmanned aerial vehicles (UAV). At high angles of attack, delta wings are capable of generating higher lift compared to conventional rectangular wings, with better aircraft stability and acute control characteristics, giving rise to higher manoeuvrability.

The flow over a delta wing at high angles of attack, α, is dominated by two large, counter-rotating leading-edge vortices (LEV) that are formed by the roll-up of vortex sheets. The flow separates from the leading edge to form a curved free shear layer above the suction side of the wing, creating a core with large axial velocity components. These large components are due to very low pressures in the vortex core, which generate additional suction and lift force on the delta wings.

However, at a sufficiently high angle of attack, these leading-edge vortices experience a sudden disorganization or state of 'burst', widely known as 'vortex breakdown' often seen on aircrafts as vapour trails. This degradable phenomenon can severely limit or even eliminate the lift gains achieved by the platform. The vortex breakdown phenomenon can be generally characterized as a rapid deceleration of both the axial and swirl components of the mean velocity and the extensive expansion of the vortex core. During the breakdown process, the mean axial velocity components rapidly decelerate into a stagnation point and/or become negative on the vortex axis. This stagnation point, identified as the 'vortex breakdown location', is unsteady and naturally fluctuates about some mean position, in the streamwise direction.

Flow fields around delta wings at moderate to high angles of attack have been examined for the past 50 years. Flow visualization techniques of Lambourne and Bryer [1] have revealed two types of vortex breakdown, i.e. the so-called 'bubble' type and the 'spiral' type of vortex breakdown. Subsequent research has shown that the *spiral* type is more common for delta wings, although occasionally, the 'bubble' type of vortex breakdown switches to the 'spiral' type from time to time in experiments. Thereafter, Srigrarom and Kurosaka [3] have decided to focus on this 'spiral' form of the breakdown, instead of the axisymmetric 'bubble' breakdown. They have formulated a theory called the Self-Induction Theory, relating to the process of vortex breakdown over delta wings and suggested surface shaping to suppress vortex breakdown on delta wings. Surface shaping by the introduction of perturbations in the form of 'bulges' gives the ability to delay or even eliminate vortex breakdown downstream of the wing. This is due to the departure of the originally linear structure of the vortex core to the wavier or 'kink' structure over these perturbations. Hence, eventually the leading edge vortex core diffuses away instead of break down, limiting the detrimental effects of vortex breakdown over an unperturbed delta wing platform.

Objective

The objectives for this experimental investigation are to explore mechanism-based control methodology to achieve radical aerodynamic gains in delta wing applications such as Unmanned Aerial Vehicle (UAV) by suppressing the performance-limiting phenomenon of vortex breakdown. In addition to that, the author will measure & analyse force/torque measurements for different suppression (perturbation) patterns and shapes of perturbation

using flow visualization to reduce or delay vortex breakdown. Eventually interpretation of data into lift and drag coefficients are conducted and analysed for each wing. Recommendation of the optimum pattern or shape of perturbation (bulges) will be discussed for each wing.

Scope

The experimental investigations are conducted at a constant freestream speed of **U** = 0.05m/s in a water tank facility in NTU. The models used in this study are delta wings with sweep angles, Λ= 60, 65 & 70°. The force measurements are only limited to the angle attack range of α = 0 to 40°, with increments of 5° in between each reading. The force measurements would be taken in 3 orthogonal axes, i.e. x, y & z directions. The focus of this study is 4 suppression patterns which have been identified initially as investigation subjects, resulting in a total of 125 sets of readings for all wings (including readings of base wing, i.e. no perturbations)**.** With optimization of the best pattern gathered from experimental results, 2 more perturbation (bulges) shapes are evaluated as basis of comparisons, i.e. "teardrop" and "diamond" perturbations, in addition to the original "round" perturbation, resulting in an additional 54 sets of readings. Dye flow visualization is conducted via a gear pump system with a singular dye probe positioned very near to the apex of each delta wing, with a constant angle of attack of α = 15° for all wings. Video recordings and still photographs would be evaluated.

Experimental Setup

Water Tunnel

The force measurements and flow visualization tests are conducted in a water tunnel facility at Nanyang Technological University (NTU) in Singapore. The cross section of the water tunnel is 0.45 x 0.6 meter square and the length of the test section is 1 meter, allowing unrestricted viewing of the model tested. The tunnel is recirculating, powered by an axial pump at the end and the maximum flow is about 0.17m/s.

General layout of Test Section

The setup of the model, together with its electrical instruments, the turntable and load cell are arranged in a manner shown below in Figure 1. The dye pump is located opposite of the electrical instruments to prevent obstruction due to its long hoses containing the dye. An illuminated board is attached at the rear side of the test section to provide clearer views of the tests conducted. A delta wing with chord length of 30cm (with its lee side facing the tester) is vertically attached by an L-shaped rod which is linked to the load cell and turntable. The vertical distance of 0.37m is chosen, so as to position the delta wing in the middle of the test section to prevent effects of boundary layer separation. The horizontal distance of 0.15m from the delta wing to the load cell is also deliberately chosen to prevent the vortices generated to affect the electronically sensitive force measurements.

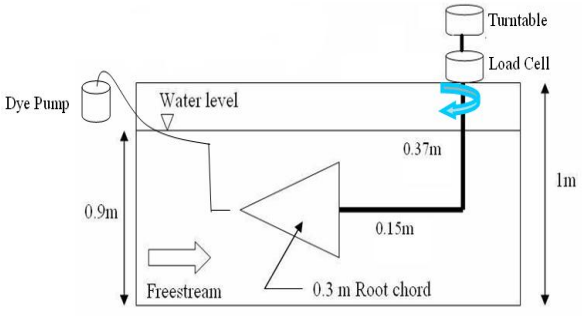

Figure 1.Schematic diagram of test section.

Wing model description

Perhaps the most important component of this study is the delta wing models itself. The clear plastic delta wing models used in this study have swept angles of 60, 65 and 70°, with sharp leading edges and bevelled at 60°. The chord length, c is 30cm and 1-centimetre intervals are marked along the root centerline. A schematic diagram of the delta wing used in the study is shown in Figure 2 below.

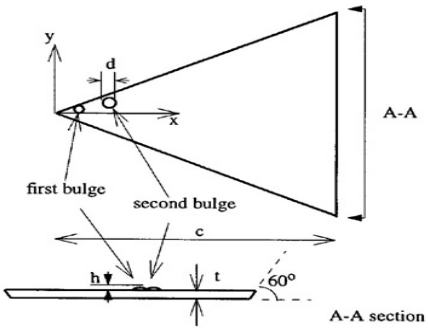

Figure 2. Schematic diagram of delta wing model used [21]

The wings used are 0.7cm thick and an L-shaped rod is mounted on the leeward side of the delta wing model at mid wingspan so that it pivots equally through the pitching range. Only the leading edge vortex closest to the tester is used in this study, i.e. the windward side.

Perturbation patterns

In this study, the author used 5 perturbation patterns incorporating the similar small and big round bulges. The 5 patterns include:

1. base wing pattern (i.e. without any bulge)
2. mild perturbation pattern, which only involves the small round bulge alone at 4cm chord length, equidistant from the root centreline
3. strong perturbation pattern with the two round bulges located along the predicted trajectory of the vortex core at 4 cm and 6cm chord length, with the small bulge nearer to the apex
4. strong perturbation *pattern A*, with the small round bulge located near the root centreline and the big round bulge located near the leading edge at 4cm and 6cm respectively
5. strong perturbation *pattern B,* with the small round bulge located near the leading edge and the big round bulge located near the root centreline at 4cm and 6cm respectively

The bulges are always attached in pairs using temporary adhesive clay for easy removal and the schematic diagram of pattern A & pattern B is illustrated below in Figure 3. The other patterns are illustrated later in Figure 7, with the omission of the base wing.

Figure 3. Schematic diagram of Pattern A (left) & Pattern B (right)

Bulge nomenclature

Another vital component of the experimental setup is the bulges that are attached on the lee side of the delta wing. The small and round bulges are used in the first stage of the tests under the 4 perturbation patterns for all delta wings. With a smooth surface, they are designed to minimize the drag effects induced by its presence itself and also to perturb the vortex core in an orderly manner. A schematic diagram showing the dimensions real of the round bulges used are presented in Figure 4.

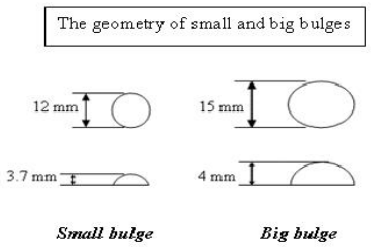

Figure 4. Schematic diagram of round bulges used

In the later stages of optimization of bulge geometry, the author has identified two more bulges with a "teardrop" and "diamond" shapes with similar dimensions to be used as perturbations. These two shapes are recommended over other geometrical shapes such as ovals or ellipse due to its sharp front end, with the potential to perturb the vortex core more effectively and cleanly. The dimensions are demonstrated in Figure 5 below.

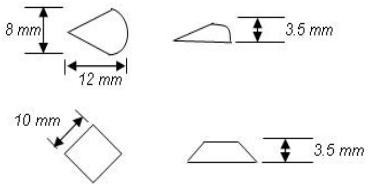

Figure 5. Schematic diagram of teardrop bulge (top), diamond bulge (bottom)

Test conditions

With favourable results obtained at low speeds as observed by Lewpiriyawong [2] in his previous studies, the tests were conducted at a low freestream speed of U=0.05m/s. This corresponds to a frequency of about 14.47Hz for the axial pump of the water tunnel. A conversion reference between the water tunnel's frequency and the actual velocity is included in the appendix section. The Reynolds number based on chord length is of 15,000. It is important to note that the water tunnel did not move water during the testing, i.e. the water level does not fluctuate about the marked level of the test section. Hence before every force measurement is started, the water is allowed to settle for a few minutes. The dye probe is located very near to the apex of the delta wing to allow diffusion of the dye on the vortex core which forms up very near at the apex leading edge. The temperature of the water in the tunnel is also kept constant.

Data Conversion

The data recorded in excel format are mere numbers with units in Newtons. It is almost impossible to evaluate or analyse the readings from force readings only. It is useful only when converted to lift and drag coefficients which are primary basis of comparisons in aerodynamics. Only through this method, the author is able to judge the reliability of the setup and instruments and also the extent of success of the bulges to perturb the vortex core by comparing with published works. The main focus of the author is the F_x, F_y and F_z readings, which are the load forces in the x, y & z directions. The lift and drag components of the delta wing are related with these 3 forces mentioned together with the angle of attack, α, by the following equations (unit in Newtons):

$$Lift, L = F_y \cos\alpha - F_x \sin\alpha$$

$$Drag, D = F_y \sin\alpha + F_x \cos\alpha$$

This is due to the orientation of the delta wing model during pitching and the pre-determined directions of x, y & z of the load cell in relation to the test section as shown below in Figure 6. The lift and drag forces are always orthogonal in aerodynamics and they are derived from similar orthogonal F_x and F_y forces measured by the load cell.

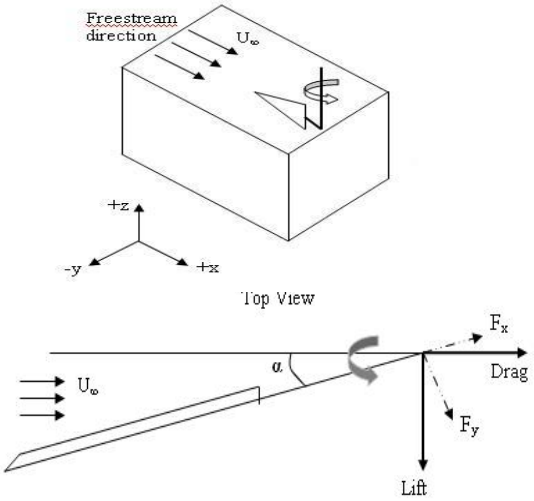

Figure 6. Schematic diagram of test section axes direction (top) & lift and drag forces on delta wing model (bottom)

The lift and drag forces derived are relatively useful in gauging of the forces acting on the model. However a very common mode of comparison for the performance in aerodynamics are the well-defined lift and drag coefficients, C_L and C_D respectively and these are used for evaluation in the next section.

Results and Discussion

60° delta wing

The 60° delta wing generally produces the highest amount of lift compared to the other two delta wing models, due to its high circulation. The mild perturbation pattern has shown the most prominent results for this particular wing, although the stall angle does not vary that much from the base wing results, as shown in Figure 8. With the optimization of the bulge geometry, the 60° delta wing significantly favours the "teardrop" bulge, providing around 10% increase in C_L throughout the range of angle of attack, as shown in Figure 9. During flow visualization, the "teardrop" bulge too manages to turn the initial straight vortex core to a very undulating one. This helps to recover the lift loss during pitching and also suppresses vortex breakdown as the linearly inductive vortices are deviated in such a manner.(Figure 10) Hence, the results of the study for the 60° delta wing clearly favour the "teardrop" bulge as its mechanism for perturbation.

65° delta wing

The 65° delta wing also produces similar results, with the mild perturbation pattern producing the highest C_L value for its case after α = 17°, during its tests (Figure 11). However, more importantly, the mild perturbation for this particular wing, manages to delay the stall angle by a further 10°. This shows that the mild perturbation is very effective for the 65° delta wing. The results from the optimization of geometry stages also indicate remarkable C_L values for the "teardrop" bulge, producing increase in C_L of more than 10% and also a delay of stall angle of more than 10° (Figure 12). Results from the flow visualization tests also reinforce the effectiveness of the "teardrop" bulge, providing the most undulating wavy vortex

core. (Figure 13) Hence a mild perturbation, utilizing the "teardrop" bulge is most suitable for the 65° delta wing.

70° delta wing

Force measurement results (Figure 14) for the 70° delta wing shows that the stagger patterns A and B are particularly ineffective in perturbation. Instead, the two patterns actually decrease the amount of lift created, resulting in very low lift coefficient values. Similarly, to the other two wings, the mild perturbation again provides good results, particularly in the range $\alpha = 20°- 30°$, providing increase of more than 10% in C_L values. The flow visualization results from the 70° delta wing rather have been rather peculiar, if compared to the other two wings. This is probably due to its small apex area, resulting in lower circulation. The "teardrop" bulges located on the 70° delta wing have only managed to perturb the vortex core slightly, resulting in a small diameter of the 'kink' structure (Figure 15); it usually produces for the other wings. On the contrary, the "diamond" bulge produces more undulation in the wavy vortex core and this is reflected in its favourable values during optimization of bulge geometry tests (Figure 16). Hence a mild perturbation, in this time round, using the "diamond" bulges is more efficient and effective.

Conclusion & Recommendations

With the exploration of the different perturbation patterns and also the three types of geometry used, the objectives of the study are clearly achieved. However, this is not an exhaustive study, as the field in flow analysis for vortex breakdown is boundless. Therefore, further improvements can still be recommended and evaluated to achieve a more comprehensive goal. Firstly, the size of the bulges has not been varied as a free variable. In other words, a smaller or bigger "teardrop" bulge may or may not produce good results for the three wings. Hence, this is a particular area that can be worked on. Finally, the location of the bulges is also not varied along the root chord line. The bulges were fixed either in the 4cm or 6cm chord mark. A further study can look into this particular matter to further improve the performance of the perturbation methodology, in line with the Self-Induction mechanism theory. Perhaps locating the bulges nearer or further away from the apex have different reactions to the linearly inductive vortices. Even more variables can be recommended in the pursuit of understanding better the roles of perturbation on the delta wing.

References

[1] Lambourne, N.C. and Bryer, D.W., "The Bursting of Leading-edge vortices-Some Observations and Discussion of the Phenomenon", ARC R&M 3282, April 1961

[2] Lewpiriyawong, N. and Srigrarom, S., "Modification of Delta wings to control vortex breakdown", Proceeding of the 12th International Symposium on Flow visualization, Gottingen, Germany, 2006

[3] Srigrarom, S. and Kurosaka, M., "Surface shaping to suppress vortex breakdown on Delta wings", *AIAA Journal*, Vol.38, No. 1, 2000

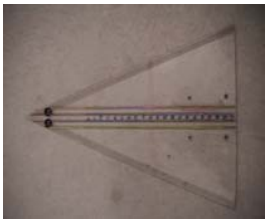

Mild perturbation

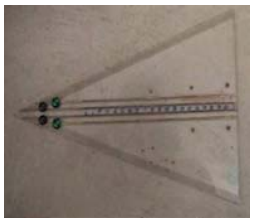

Strong perturbation (along trajectory)

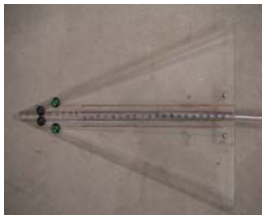

Strong perturbation pattern A

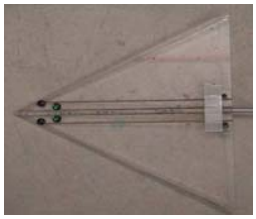

Strong perturbation pattern B

Figure 7. Actual perturbation patterns of round bulges

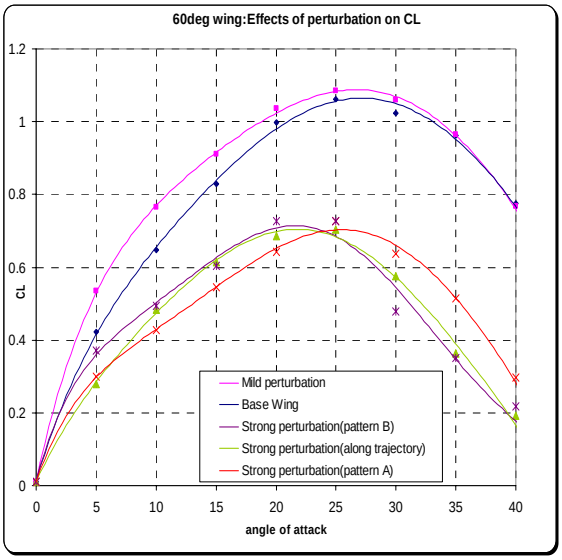

Figure 8. Lift coefficient of 60° wing for 5 perturbation patterns

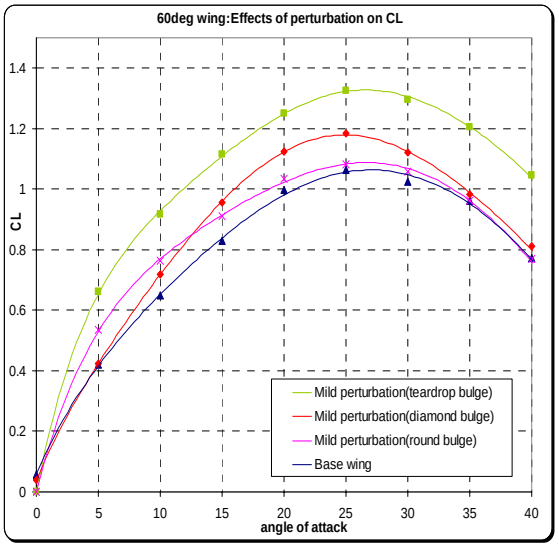

Figure 9. Lift coefficient of 60° wing for 3 types of bulge geometry

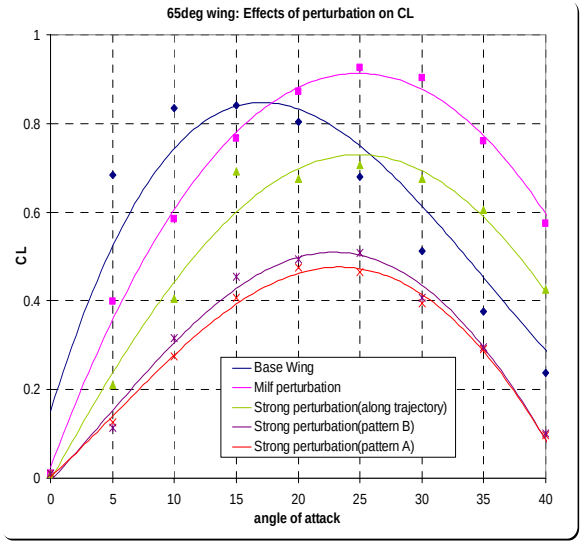

Figure 11. Lift coefficient of 65° wing for 5 perturbation patterns

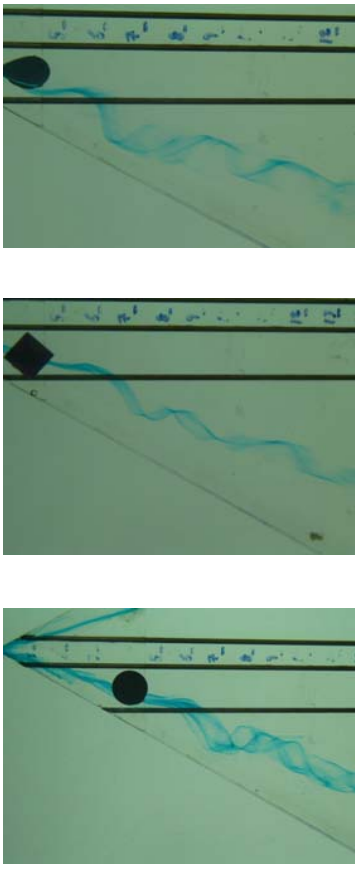

Figure 10. Visualization result of 3 different bulge geometry on 60° wing

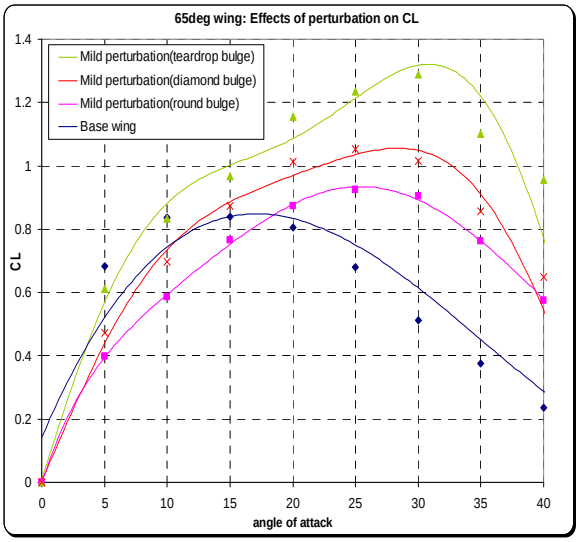

Figure 12. Lift coefficient of 65° wing for 3 types of bulge geometry

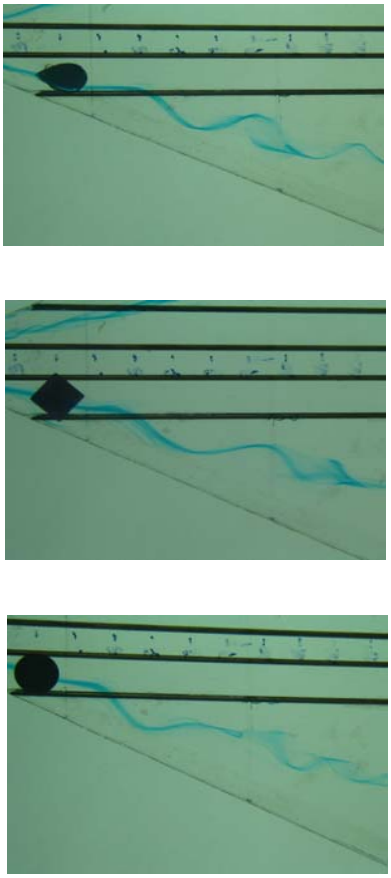

Figure 13. Visualization result of 3 different bulge geometry on 65° wing

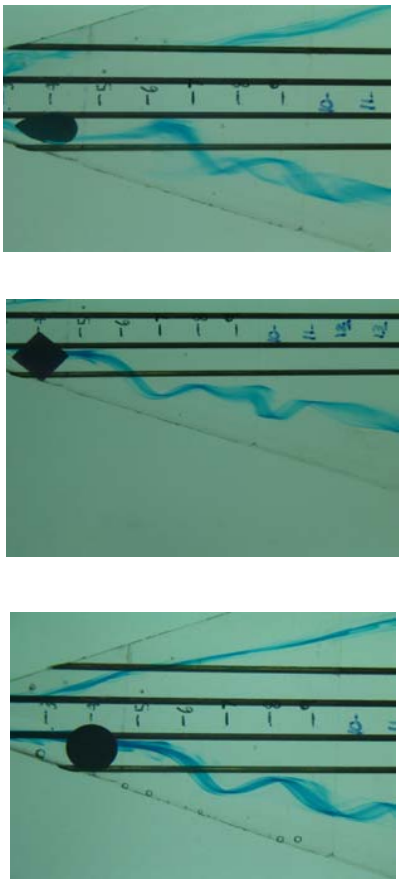

Figure 15. Visualization result of 3 different bulge geometry on 70° wing

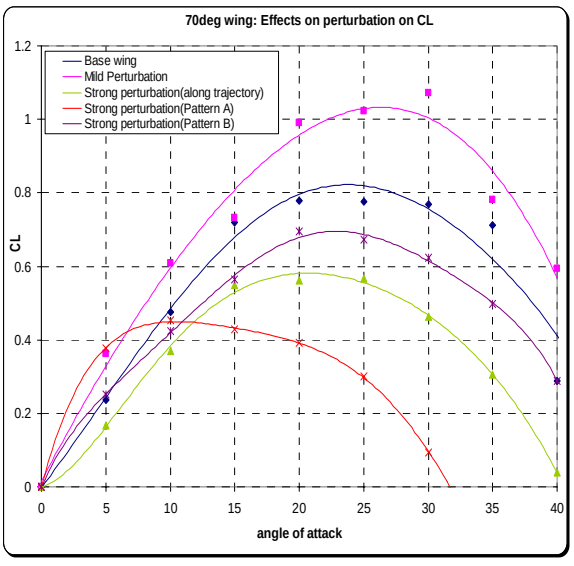

Figure 14. Lift coefficient of 70° wing for 5 perturbation patterns

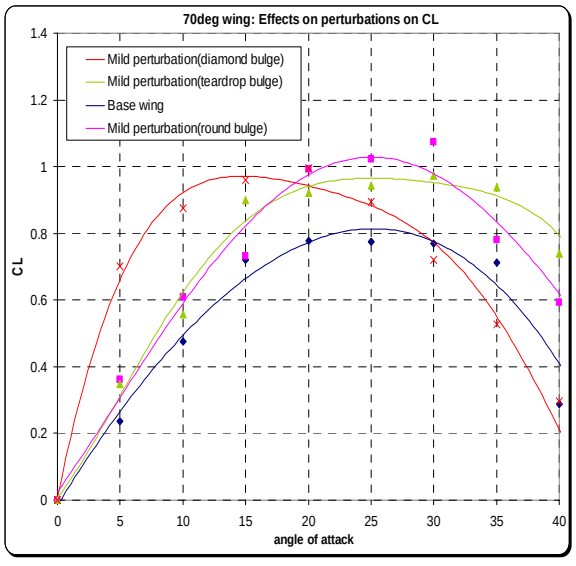

Figure 16. Lift coefficient of 70° wing for 3 types of bulge geometry